ACS OMEGA

Open Access

http://pubs.acs.org/journal/acsodf

Article

σ-Hole Site-Based Interactions within Hypervalent Pnicogen, Halogen, and Aerogen-Bearing Molecules with Lewis Bases: A Comparative Study

Mahmoud A.A. Ibrahim,* Asmaa M.M. Mahmoud, Mohammed N.I. Shehata, Rehab R.A. Saeed, Nayra A.M. Moussa, Shaban R.M. Sayed, Mohamed Khaled Abd El-Rahman, and Tamer Shoeib*

Cite This: *ACS Omega* 2024, 9, 10391−10399

Read Online

ACCESS | Metrics & More | Article Recommendations

ABSTRACT: σ-Hole site-based interactions in the trigonal bipyramidal geometrical structure of hypervalent pnicogen, halogen, and aerogen-bearing molecules with pyridine and NCH Lewis bases (LBs) were comparatively examined. In this respect, the $ZF_5\cdots$, $XF_3O_2\cdots$, and $AeF_2O_3\cdots$LB complexes (where Z = As, Sb; X = Br, I; Ae = Kr, Xe; and LB = pyridine and NCH) were investigated. The electrostatic potential (EP) analysis affirmations outlined the occurrence of σ-holes on the systems under consideration with disparate magnitudes that increased according to the following order: $AeF_2O_3 < XF_3O_2 < ZF_5$. In line with EP outcomes, the proficiency of σ-hole site-based interactions increased as the atomic size of the central atom increased with a higher favorability for the pyridine-based complexes over NCH-based ones. The interaction energy showed the most favorable negative values of −35.97, −44.53, and −56.06 kcal/mol for the $XeF_2O_3\cdots$, $IF_3O_2\cdots$, and $SbF_5\cdots$pyridine complexes, respectively. The preferentiality pattern of the studied interactions could be explained as a consequence of (i) the dramatic rearrangement of ZF_5 molecules from the trigonal bipyramid geometry to the square pyramidal one, (ii) the significant and tiny deformation energy in the case of the interaction of XF_3O_2 molecules with pyridine and NCH, respectively, and (iii) the absence of geometrical deformation within the $AeF_2O_3\cdots$pyridine and ⋯NCH complexes other than the $XeF_2O_3\cdots$pyridine one. Quantum theory of atoms in molecules and noncovalent interaction index findings reveal the partially covalent nature of most of the investigated interactions. Symmetry−adapted perturbation theory affirmations declared that the electrostatic component was the driving force beyond the occurrence of the considered interactions. The obtained findings will help in improving our understanding of the effect of geometrical deformation on intermolecular interactions.

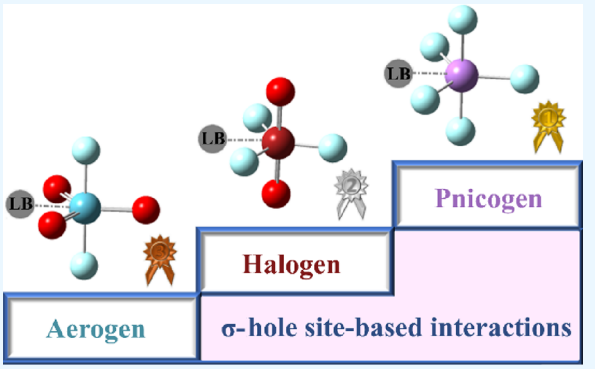

INTRODUCTION

Noncovalent interactions have been stated to play a substantial role in various chemical and biochemical processes.[1−9] In particular, σ-hole interactions have received considerable attention over the past decade because of their unique contributions to crystal materials,[10−14] biological systems,[15−18] and catalysis.[19] The first σ-hole conceptualization was described as a region suffering from a lack of electron density along the σ-bond of the group VII element-containing molecules.[20] The σ-hole term was then extended until it encompassed the group IV−VIII elements. The interactions of the so-called σ-hole of the abovementioned groups with a Lewis base led to form tetrel,[21−24] pnicogen,[25−30] chalcogen,[31−37] halogen,[38−42] and aerogen[43−45] bonds, respectively.

In the literature, the favorability of the σ-hole interaction was denoted to be affected by various factors, comprising the atomic size of the σ-hole donor atom and the electron-withdrawing power of its attached atom.[46,47] It is worth mentioning that geometrical deformation plays a significant role in magnifying these interactions. As a point of departure, the effect of geometrical deformation was adequately assessed within the interactions of the tetrel-bearing molecules in the fashion of the tetrahedral geometry.[48−50] Subsequently, the hypervalent pnicogen-, chalcogen-, and halogen-bearing molecules were addressed with an outstanding geometrical deformation effect on their interactions with LBs.[51] It is worth mentioning that the trigonal bipyramidal geometry of the pnicogen-bearing molecules in their complexed form was

Received: October 18, 2023
Revised: January 2, 2024
Accepted: January 22, 2024
Published: February 23, 2024

recorded with the highest interaction energy in comparison to the seesaw/octahedral and square pyramidal of the chalcogen- and halogen-bearing ones, respectively. Such preferentiality could be attributed to the geometrical deformation of the ZF_5 molecule (where Z = P, As, and Sb) from a trigonal bipyramidal geometry to a square pyramidal counterpart, which is accompanied by a larger σ-hole size.[52,53] However, the deformation effect on the trigonal bipyramidal geometry of the halogen and aerogen-bearing molecules through their interactions with LBs has not yet been studied yet.

In this regard, the ability of halogen- and aerogen-bearing molecules within a trigonal bipyramidal geometry to engage in σ-hole site-based interactions with LBs was thoroughly studied and then compared with the previously reported pnicogen-bearing analogues. For this aim, ZF_5···, XF_3O_2···, and AeF_2O_3··· pyridine/NCH complexes were investigated (Figure 1). The

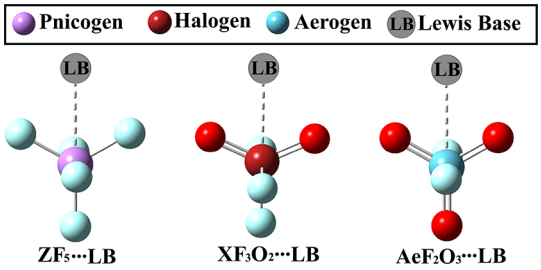

Figure 1. Illustrative representation of the investigated pnicogen-(ZF_5)/halogen(XF_3O_2)/aerogen(AeF_2O_3)···Lewis base (LB) complexes (where Z = As and Sb; X = Br and I; Ae = Kr and Xe; and LB = pyridine and NCH).

presented work will open up a wide range of research on hypervalent noncovalent interactions, leading to a more significant improvement in their applications in anion recognition, biological systems, and crystal engineering.

COMPUTATIONAL METHODS

Various ab initio calculations were conducted to comparatively study the σ-hole site-based interactions of hypervalent pnicogen, halogen, and aerogen-bearing molecules with LBs using Gaussian 09 software.[54] In this regard, the ZF_5, XF_3O_2, and AeF_2O_3 molecules (where Z = As and Sb; X = Br and I; and Ae = Kr and Xe) within the trigonal bipyramidal geometry were devoted to directly interacting with pyridine and NCH molecules. All the systems under study were optimized at the MP2/aug-cc-pVTZ level of theory except for the Z, X, and Ae atoms.[55−57] The pseudopotentials (PPs) were treated for the aforementioned excluded atoms for the relativistic effect considerations.[58]

The electrostatic potential (EP) analysis was performed for the optimized ZF_5, XF_3O_2, and AeF_2O_3 molecules using a 0.002 a.u. electron density envelope upon previous recommendations, owing to its deserving representation for the surfaces of chemical systems.[59] Molecular electrostatic potential (MEP) maps were accordingly visualized to illustrate the nucleophilic and electrophilic regions accompanied by evaluation of the maximum positive electrostatic potential ($V_{s,max}$) values.

Upon the optimized $ZF_5/XF_3O_2/AeF_2O_3$···pyridine/NCH complexes, the interaction energy (E_{int}) was assessed as the variation between the complex's energy and the sum of its monomer within their complexation geometry (eq 1), while binding energies (E_{bind}) were computed as the energy produced by subtracting the sum of the optimized monomers' energies from the complex's energy, as demonstrated in eq 2.[60] The basis set superposition error (BSSE) was eliminated by considering the counterpoise correction method.[61] The deformation energy (E_{def}) was also enumerated as the variation between the E_{bind} and E_{int}, as given in eq 3.[62]

$$E_{int} = E_{\text{Lewis acid}\cdots\text{Lewis base}} - (E_{\text{Lewis acid in complex}} + E_{\text{Lewis base in complex}}) + E_{BSSE} \quad (1)$$

$$E_{bind} = E_{\text{Lewis acid}\cdots\text{Lewis base}} - (E_{\text{Lewis acid}} + E_{\text{Lewis base}}) + E_{BSSE} \quad (2)$$

$$E_{def} = E_{bind} - E_{int} \quad (3)$$

Moreover, the nature of the studied interactions was unveiled using the quantum theory of atoms in molecules (QTAIM)[63] along with the noncovalent interaction (NCI) index analyses.[64] The EP, QTAIM, and NCI analyses were executed through the Multiwfn 3.7 package.[65] The QTAIM schemes and NCI plots were built using Visual Molecular Dynamics software.[66] Symmetry−adapted perturbation theory (SAPT) analysis was accomplished to illustrate the physical nature of the inspected interactions.[67] SAPT calculations were proceeded at the SAPT2+(3)dMP2 level of truncation via a PSI4 code[68] to assess the fundamental energetic terms into dispersion (E_{disp}), exchange (E_{exch}), electrostatic (E_{elst}), and induction (E_{ind}) energies. The total SAPT2+(3)dMP2 energy ($E_{SAPT2+(3)dMP2}$) was given via eq 4.[69]

$$E_{int}^{SAPT2+(3)dMP2} = E_{elst} + E_{ind} + E_{disp} + E_{exch} \quad (4)$$

RESULTS AND DISCUSSION

EP Analyses. EP analyses were employed to visualize and evaluate the electron-deficient/rich regions over the molecular systems by generating MEP maps and $V_{s,max}$ values for the ZF_5, XF_3O_2, and AeF_2O_3 molecules (Figure 2).

Inspecting the displayed MEP maps, the occurrence of the blue-coded region (i.e., σ-hole) was denoted with variable sizes (Figure 2) along the extension of the F-Z, F-X, and O-Ae covalent bonds for ZF_5, XF_3O_2, and AeF_2O_3, respectively. These findings confirmed the noticeable versatility of the examined molecules to engage in σ-hole interactions. Notably, the σ-hole size was detected to increase by going from the AeF_2O_3 molecules to XF_3O_2 and ZF_5 ones, which could be interpreted as a consequence of the higher polarizability of the heavier atoms.

Turning to $V_{s,max}$ affirmations, the σ-hole magnitude was denoted with observable increase according to the following order AeF_2O_3 < XF_3O_2 < ZF_5 molecules. For instance, the $V_{s,max}$ values of the XeF_2O_3, IF_3O_2, and SbF_5 molecules were 45.2, 57.6, and 79.1 kcal/mol, respectively. In line with MEP outcomes, an increase in $V_{s,max}$ values were observed for the heavier atoms with values up to 33.6 and 45.2 kcal/mol for KrF_2O_3 and XeF_2O_3 molecules, respectively.

Interaction Energy. σ-Hole site-based interactions among the hypervalent ZF_5, XF_3O_2, and AeF_2O_3 molecules in the trigonal bipyramidal geometry and the utilized LBs were intensively studied. Geometry optimization calculations were carried out for $ZF_5/XF_3O_2/AeF_2O_3$···pyridine/NCH, and the obtained structures are given in Figure 3. Upon the optimized

https://doi.org/10.1021/acsomega.3c08178
ACS Omega 2024, 9, 10391−10399

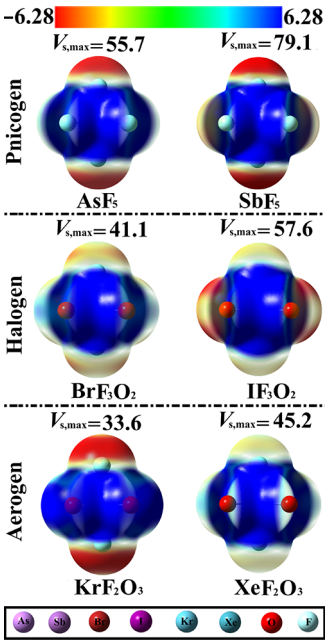

Figure 2. Distributions of charge over the entities of the hypervalent pnicogen (ZF_5), halogen (XF_3O_2), and aerogen (AeF_2O_3)-bearing molecules (where Z= As and Sb; X = Br and I; and Ae = Kr and Xe). EP varies from −6.28 (red) to 6.28 (blue) kcal/mol. Values of $V_{s,max}$ are given in kcal/mol.

geometries, the E_{int}, E_{bind}, and E_{def} values were computed and are gathered in Table 1. The correlation between the E_{int} of the studied complexes and $V_{s,max}$ values of their deformed monomers was graphed (Figure 4).

As illustrated in Figure 3, the optimized structures demonstrated the significant effect of the deformation process that was noticed in the investigated σ-hole site-based interactions within almost all of the studied complexes. Moreover, the optimum distances were denoted to be less than the sum of the corresponding van der Waals radii, affirming the evident ability of the $ZF_5/XF_3O_2/AeF_2O_3$ molecules to engage in the investigated interactions. Meanwhile, the percentage (%) of the sum of the corresponding covalent radii ($\sum r_{covalent}$) values emphasized that the obtained complexes would not have covalent bonding features, only a partially covalent or noncovalent nature.

Inspecting the change in the θ_2 angles of the $ZF_5/XF_3O_2/AeF_2O_3$ molecules after complexation with Lewis bases, noticeable deformation in the trigonal bipyramidal structures was obtained with disparate degrees relying on the central atom in the investigated interactions (Figure 3). Detailedly, a drastic deformation of the ZF_5 geometries from the trigonal bipyramid structure to the square pyramidal one was denoted upon complexation of the pnicogen-bearing molecules with the pyridine and NCH LBs, enabling the ZF_5 molecules to efficiently engage in opulent σ-hole site-based interactions. As evident in Table 1, considerable E_{def} values were obtained within an energetic range of 6.87−21.50 kcal/mol.

Regarding the halogen-bearing complexes, significant E_{def} was observed in the case of $XF_3O_2\cdots$pyridine complexes only with E_{def} values up to 26.22 and 18.49 kcal/mol, where X = Br and I, respectively. Subsequently, the geometrical structure of the XF_3O_2 molecules within the aforementioned complexes mimicked the rearrangement relevant to the pnicogen-bearing counterparts. In comparison, small E_{def} values of 0.19 and 3.06 kcal/mol were found in the case of the $BrF_3O_2\cdots$ and $IF_3O_2\cdots$

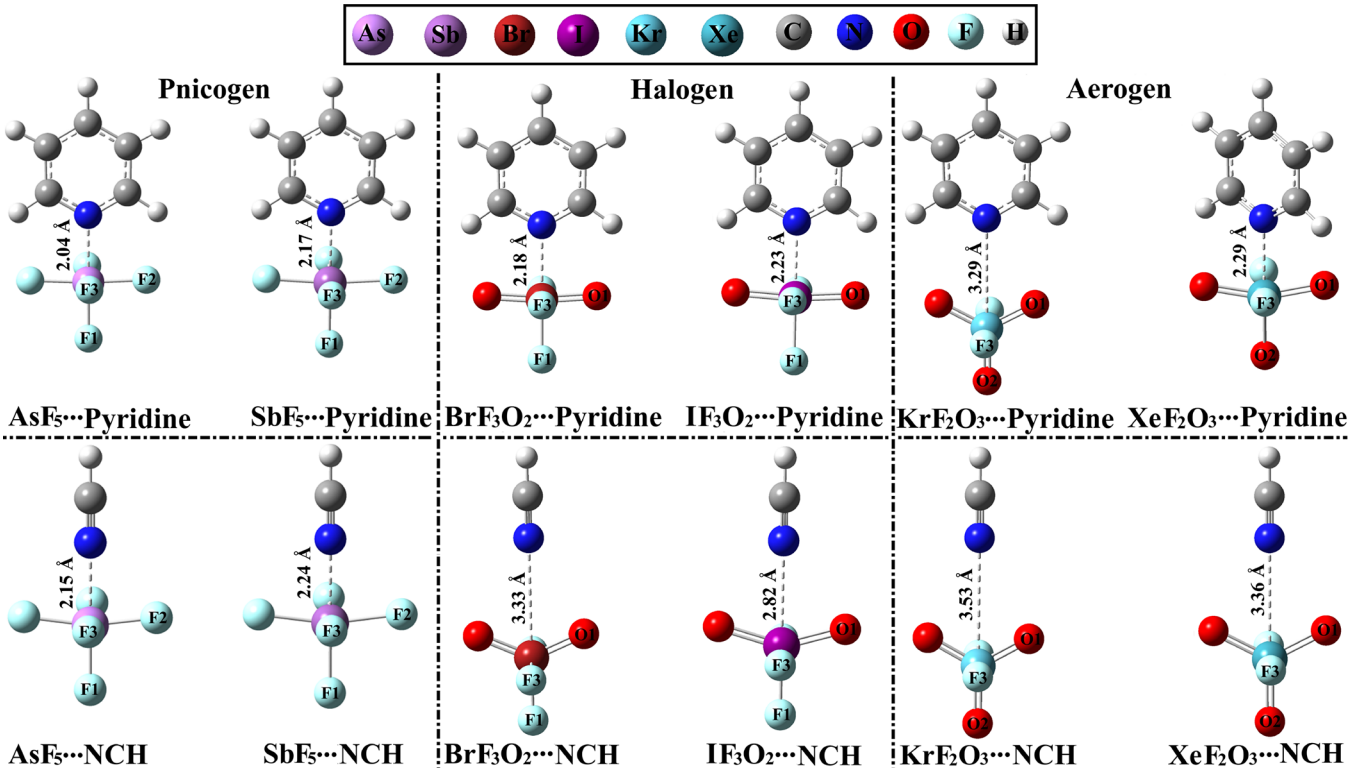

Figure 3. Optimized structures of the pnicogen(ZF_5)/halogen(XF_3O_2)/aerogen(AeF_2O_3)···Lewis base (LB) complexes (where Z = As and Sb; X = Br and I; Ae = Kr and Xe; and LB = pyridine and NCH).

https://doi.org/10.1021/acsomega.3c08178
ACS Omega 2024, 9, 10391−10399

Table 1. Computed Values of E_{int}, E_{bind}, and E_{def} (in kcal/mol) for the Optimized Pnicogen (ZF_5)/Halogen (XF_3O_2)/Aerogen (AeF_2O_3)···Lewis Base (LB) Complexes (where Z = As and Sb; X = Br and I; Ae = Kr and Xe; and LB = Pyridine and NCH)

	complex	distance (Å)	%of $\sum r_{covalent}$ [a]	θ_1 [b] (deg)	θ_2 [c] (deg)	E_{int}	E_{bind}	E_{def} [d]	$V_{s,max}$
pnicogen	AsF_5···pyridine	2.04	108	179.99	89.82	−52.39	−30.89	21.50	131.5
	SbF_5···pyridine	2.17	105	179.99	89.71	−56.06	−40.20	12.86	153.0
	AsF_5···NCH	2.15	114	179.99	89.15	−19.22	−9.52	19.22	122.2
	SbF_5···NCH	2.24	108	179.99	89.11	−26.55	−19.68	6.87	147.1
halogen	BrF_3O_2···pyridine	2.18	115	179.99	89.90	−32.61	−6.39	26.22	76.6
	IF_3O_2···pyridine	2.23	107	180.00	89.89	−44.53	−26.04	18.49	92.2
	BrF_3O_2···NCH	3.33	176	180.00	92.97	−2.55	−2.36	0.19	44.5
	IF_3O_2···NCH	2.82	136	180.00	91.46	− 7.04	−3.98	3.06	74.4
aerogen	KrF_2O_3···pyridine	3.29	151	179.99	89.72	−3.85	−3.37	0.48	39.7
	XeF_2O_3···pyridine	2.29	105	179.99	88.39	−35.97	−13.33	22.64	93.1
	KrF_2O_3···NCH	3.53	162	179.99	89.94	−2.04	−1.93	0.11	36.6
	XeF_2O_3···NCH	3.36	154	179.99	89.65	−2.84	−2.28	0.56	52.6

[a]% of $\sum r_{covalent}$ represents the percentage of the sum of the corresponding covalent radii ($\sum r_{covalent}$). [b]θ_1 represents ∠F1−Z/X···N and ∠O2−Ae···N within the optimized ZF_5/XF_3O_2··· and AeF_2O_3···LB complexes, respectively (see Figure 3). [c]θ_2 represents ∠F2−Z−F3 and ∠O1−X/Ae−F3 within the ZF_5 and XF_3O_2/AeF_2O_3 molecules, respectively (see Figure 3). [d]$V_{s,max}$ of the deformed structures of the ZF_5, XF_3O_2, and AeF_2O_3 monomers are given in kcal/mol.

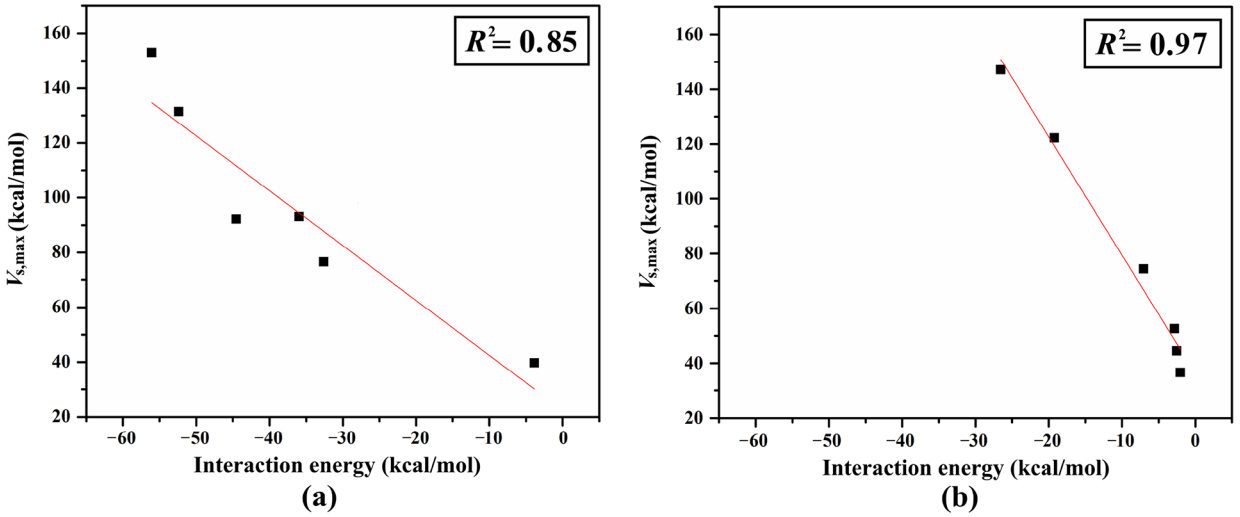

Figure 4. Correlation between the interaction energy (E_{int}) of the optimized pnicogen(ZF_5)/halogen(XF_3O_2)/aerogen(AeF_2O_3)···Lewis base (LB) complexes (where Z = As and Sb; X = Br and I; Ae = Kr and Xe; and LB = pyridine and NCH) and $V_{s,max}$ values of their deformed monomers. (a, b) Pyridine-based and NCH-based complexes, respectively.

NCH complexes with a slight change in the XF_3O_2 trigonal bipyramid geometry.

Turning to aerogen-bearing complexes, tiny E_{def} values were observed for the studied complexes except for the XeF_2O_3··· pyridine complex. Such an observation outlined an inconspicuous change of the geometrical structure of the AeF_2O_3 molecules upon complexation with either the pyridine or NCH LBs regardless of the XeF_2O_3···pyridine complex.

As a consequence of the preceding observations, the strength of σ-hole site-based interactions was detected to increase with significant E_{int} and E_{bind} values in the posterior pattern: AeF_2O_3 < XF_3O_2 < ZF_5···pyridine/NCH complexes (Table 1). The E_{int} energies of the investigated complexes were generally consistent with $V_{s,max}$ values of the deformed monomers, giving correlation coefficient (R^2) values of 0.85 and 0.97 in the case of the pyridine and NCH-based complexes, respectively (Figure 4). Evidently, the E_{int} energies were −2.84, −7.04, and −26.55 kcal/mol for XeF_2O_3···, IF_3O_2···, and SbF_5···NCH complexes along with $V_{s,max}$ values of 52.6, 74.4, and 147.1 kcal/mol for their deformed XeF_2O_3, IF_3O_2, and SbF_5 monomers, respectively (Table 1).

Additionally, negative values of E_{int} and E_{bind} increased with increasing the atomic size of the inspected pnicogen, halogen, and aerogen atoms. For instance, the E_{int}/E_{bind} values of the BrF_3O_2··· and IF_3O_2···pyridine complexes were −32.61/−6.39 and −44.53/−26.04 kcal/mol, respectively. Conspicuously, higher E_{int}/E_{bind} values were observed for the pyridine-based complexes compared to the NCH analogues. Impressively, optimum intermolecular distances were disclosed to be directly correlated with energetic trends, where the studied interactions were enhanced by decreasing the intermolecular distances. Illustratively, the XeF_2O_3···, IF_3O_2···, and SbF_5···NCH complexes were characterized by E_{int}/E_{bind} values of −2.84/−2.28, − 7.04/−3.98, and −26.55/−19.68 kcal/mol at optimum intermolecular distances of 3.36, 2.82, and 2.24 Å, respectively.

QTAIM Analysis. Toward more validation for the occurrence of noncovalent interactions, QTAIM analysis was implemented.[70,71] Diagrams of QTAIM relevant to the optimized $ZF_5/XF_3O_2/AeF_2O_3$···pyridine/NCH complexes

https://doi.org/10.1021/acsomega.3c08178
ACS Omega 2024, 9, 10391−10399

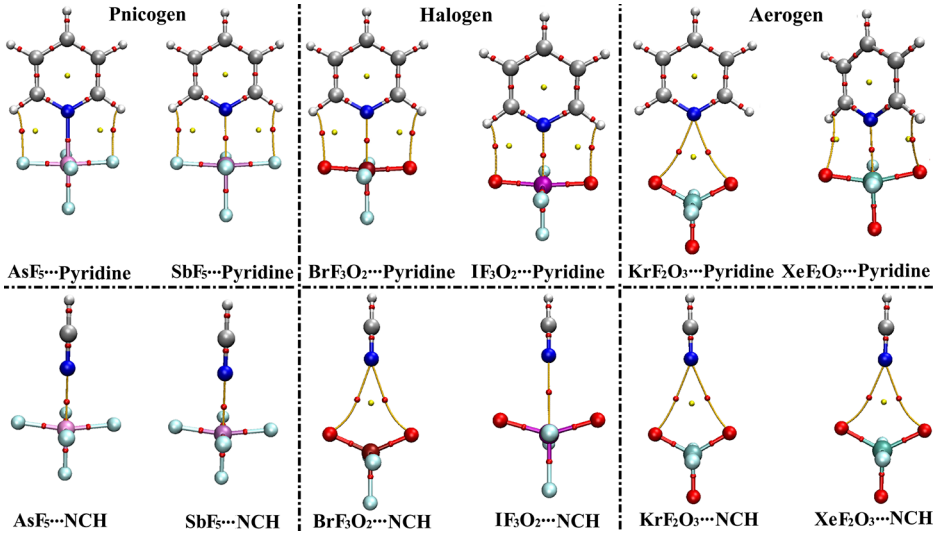

Figure 5. Diagrams of QTAIM relevant to the optimized pnicogen(ZF_5)/halogen(XF_3O_2)/aerogen(AeF_2O_3)···Lewis base (LB) complexes (where Z = As and Sb; X = Br and I; Ae = Kr and Xe; and LB = pyridine and NCH). Red dots indicate the locations of the BPs and BCPs. The small red and yellow dots represent bond critical points (BCPs) and ring critical points (RCPs), respectively.

Table 2. Topological Parameters (in a.u.), Including ρ_b, $\nabla^2\rho_b$, and H_b, at BCPs of the Optimized Pnicogen(ZF_5)/Halogen(XF_3O_2)/Aerogen(AeF_2O_3)···Lewis Base (LB) Complexes (where Z = As and Sb; X = Br and I; Ae = Kr and Xe; and LB = Pyridine and NCH)

complex		ρ_b	$\nabla^2\rho_b$	H_b
pnicogen	AsF_5···pyridine	0.0718	0.0718	−0.0612
	SbF_5···pyridine	0.0918	0.1895	−0.0373
	AsF_5···NCH	0.0678	0.1236	−0.0251
	SbF_5···NCH	0.0679	0.1991	−0.0184
halogen	BrF_3O_2···pyridine	0.0981	0.0337	−0.0397
	IF_3O_2···pyridine	0.2164	0.4931	−0.1687
	BrF_3O_2···NCH	0.0082	0.0316	0.0015
	IF_3O_2···NCH	0.0245	0.0691	0.0001
aerogen	KrF_2O_3···pyridine	0.0115	0.0436	0.0018
	XeF_2O_3···pyridine	0.0936	0.0271	−0.0409
	KrF_2O_3···NCH	0.0069	0.0273	0.0015
	XeF_2O_3···NCH	0.0095	0.0360	0.0017

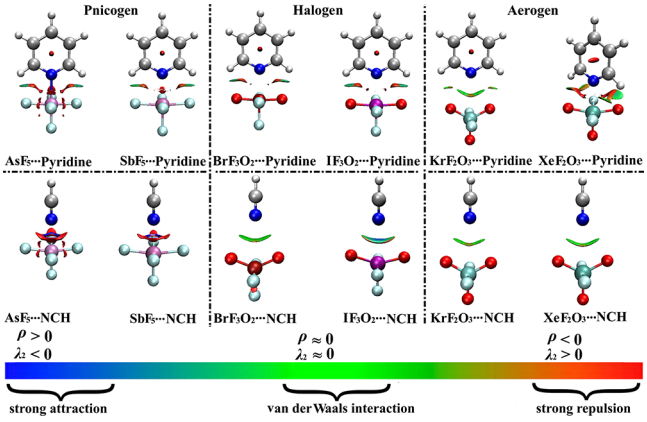

Figure 6. 3D NCI diagrams of the optimized pnicogen(ZF_5)/halogen(XF_3O_2)/aerogen(AeF_2O_3)···Lewis base (LB) complexes (where Z = As and Sb; X = Br and I; Ae = Kr and Xe; LB = pyridine and NCH).

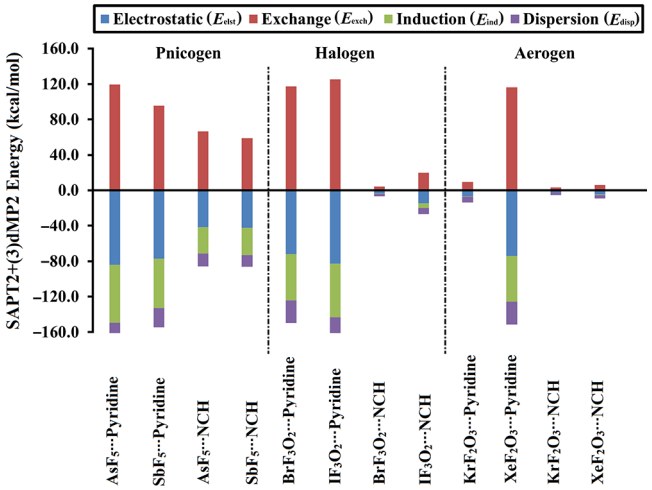

Figure 7. Bar chart of the four physical energetic components for the optimized pnicogen(ZF_5)/halogen(XF_3O_2)/aerogen(AeF_2O_3)··· Lewis base (LB) complexes (where Z = As and Sb; X = Br and I; Ae = Kr and Xe; and LB = pyridine and NCH).

are graphed in Figure 5. The corresponding topological parameters, encompassing the $\nabla^2\rho_b$, H_b, and ρ_b, were computed and are enrolled in Table 2.

According to Figure 5, the existence of σ-hole site-based interactions was confirmed within the pnicogen-bearing complexes via the appearance of a single BCP and BP between the Z atom and the Lewis base. Additionally, two BCPs and BPs were disclosed in the case of ZF_5···pyridine complexes, indicating the occurrence of hydrogen bonds. The same findings were found within the halogen-bearing complexes other than that of the BrF_3O_2···NCH complex. The interactions within the latter complex were characterized by the existence of secondary interactions between the oxygen atoms and the Lewis base.

Turning to aerogen-bearing complexes, two BPs and BCPs were observed between the oxygen atoms and the N atom of the Lewis base with an exception for the XeF_2O_3···pyridine complex. For the latter exceptional complex, three BCPs and

https://doi.org/10.1021/acsomega.3c08178
ACS Omega 2024, 9, 10391−10399

Table 3. E_{elst}, E_{ind}, E_{disp}, E_{exch}, and $E_{SAPT2+(3)dMP2}$ (in kcal/mol) along the Energy Difference ($\Delta\Delta E$) between the MP2 and SAPT2+(3)dMP2 Energies of the Optimized Pnicogen(ZF_5)/Halogen(XF_3O_2)/Aerogen(AeF_2O_3)···Lewis Base (LB) Complexes (where Z = As and Sb; X = Br and I; Ae = Kr and Xe; and LB = Pyridine and NCH)

complex		E_{elst}	E_{ind}	E_{disp}	E_{exch}	$E_{SAPT2+(3)dMP2}$[a]	$\Delta\Delta E$[b]
pnicogen	AsF_5···pyridine	−84.13	−65.18	−25.03	119.62	−54.71	−2.32
	SbF_5···pyridine	−77.30	−55.48	−21.80	95.44	−59.14	−3.08
	AsF_5···NCH	−41.71	−29.75	−14.27	66.44	−19.28	−0.06
	SbF_5···NCH	−42.50	−30.52	−13.20	59.11	−27.11	−0.56
halogen	BrF_3O_2···pyridine	−71.89	−52.53	−25.38	117.43	−32.37	0.24
	IF_3O_2···pyridine	−82.58	−60.77	−26.56	125.24	−44.68	−0.15
	BrF_3O_2···NCH	−3.45	−0.37	−3.04	4.37	−2.48	0.07
	IF_3O_2···NCH	−14.71	−5.07	−6.89	19.63	−7.04	0.00
aerogen	KrF_2O_3···pyridine	−6.77	−0.42	−6.38	9.51	−4.06	−0.21
	XeF_2O_3···pyridine	−74.15	−51.49	−25.83	116.58	−34.90	1.07
	KrF_2O_3···NCH	−2.39	−0.19	−2.69	3.27	−2.00	0.04
	XeF_2O_3···NCH	−4.72	−0.49	−3.74	6.05	−2.90	−0.06

[a] $E_{SAPT2+(3)dMP2} = E_{ind} + E_{exch} + E_{elst} + E_{disp}$ [b] $\Delta\Delta E = E_{MP2/aug-cc-pVTZ(PP)} - E_{SAPT2=(3)dMP2}$

BPs were observed: one for the σ-hole site-based interactions and two for hydrogen bonds. Accordingly, the strong contribution of the σ-hole···N interaction to the overall strength of the XeF_2O_3···pyridine complex was outlined. While no evidence for the contribution of the latter interaction was observed within the XeF_2O_3···NCH and KrF_2O_3··· pyridine/NCH complexes. This observation was consistent with the previously documented emphasis on the BPs' minimal significance in determining the origin of the interactions under consideration.[72,73]

From Table 2, high positive ρ_b values along with negative H_b values were denoted for the pnicogen-bearing complexes, parading their partially covalent character. In parallel, the same findings were observed for the XF_3O_2··· and XeF_2O_3···pyridine complexes. This finding demonstrated the significant effect of the deformation process on enhancing the investigated interactions. Unlike the prior findings, positive signs of ρ_b and H_b with low values were detected for the other complexes, illustrating their closed-shell nature. Generally, the topological parameter trends were in sync with the energetic pattern. Evidently, noticeable ρ_b, $\nabla^2\rho_b$, and H_b values were detected for the ZF_5/XF_3O_2/AeF_2O_3···pyridine complexes over the ZF_5/XF_3O_2/AeF_2O_3···NCH complexes. For instance, ρ_b values of SbF_5···pyridine and ···NCH complexes were 0.0918 and 0.0679 a.u. along with E_{int}/E_{bind} values of −56.06/−40.20 and −26.55/−19.68 kcal/mol, respectively.

NCI Analysis. The NCI index has previously been described as a powerful tool for detecting the presence of closed- and open-shell interactions.[74] NCI plots were built for the ZF_5/XF_3O_2/AeF_2O_3···pyridine/NCH complexes by using a reduced density gradient value of 0.50 a.u. (Figure 6).

As evident in Figure 6, empty areas surrounded by blue/red circles were observed within the ZF_5···pyridine/NCH, XF_3O_2···pyridine, and XeF_2O_3···pyridine complexes, reflecting their partially covalent bonding nature. Regarding XF_3O_2··· NCH complexes, NCI findings showed the existence of blue-colored surfaces, addressing the occurrence of a strong intermolecular attractive interaction. Apparently, greenish-red and brownish-red areas within the AeF_2O_3···pyridine/NCH complexes were observed, revealing the existence of van der Waals attraction and repulsive forces, respectively. These results were in line with the QTAIM outlines.

SAPT Calculations. SAPT analysis has been developed as a reliable tool for elucidating the driving force that plays a significant role in intermolecular interactions.[75] For the optimized ZF_5/XF_3O_2/AeF_2O_3···LB complexes, the attractive and repulsive energetic components are graphed in Figure 7 and Table 3.

Manifestly, in Figure 7, the E_{elst} component was detected with predominant contributions in the investigated interactions within the ZF_5/XF_3O_2/AeF_2O_3···pyridine/NCH complexes except for the KrF_2O_3···NCH complex that was dominated by the E_{disp}. Additionally, significant contributions to the E_{ind} and E_{disp} were also denoted. The obtained negative values of the abovementioned energetic components manifested the role of their attractive nature in stabilizing all ZF_5/XF_3O_2/AeF_2O_3···pyridine/NCH complexes. Unlike the prior components, E_{exch} was announced as a repulsive one with high positive values. For instance, the E_{elst}, E_{ind}, E_{disp}, and E_{exch} of the SbF_5···pyridine complex were −77.30, − 55.48, − 21.80, and 95.44 kcal/mol, respectively (Table 3).

As listed in Table 3, growing contributions of the attractive forces to the studied interactions within the ZF_5···pyridine/NCH, XF_3O_2···pyridine, and XeF_2O_3···pyridine complexes were noticed to follow the $E_{disp} < E_{ind} < E_{elst}$ sequence. For the other complexes, the attractive energetic components of the interactions were generally aligned following the $E_{ind} < E_{disp} < E_{elst}$ order. For instance, E_{elst}, E_{ind}, and E_{disp} of the SbF_5··· pyridine complex were −77.30, −55.48, and −21.80 kcal/mol, respectively.

Further, a notable agreement was observed between the $E_{SAPT2+(3)dMP2}$, E_{int}, and $V_{s,max}$ values of all of the investigated systems. For instance, $E_{SAPT2+(3)dMP2}$ were −59.14, − 44.68, and −34.90 kcal/mol for the SbF_5···, IF_3O_2···, and XeF_2O_3··· pyridine complexes that exhibited E_{int} values of −56.06, − 44.53, and −35.97 kcal/mol, accompanied by $V_{s,max}$ values of 79.1, 57.6, and 45.2 kcal/mol for the SbF_5, IF_3O_2, and XeF_2O_3 molecules, respectively.

The reliability of the incorporated SAPT level was confirmed via the tiny $\Delta\Delta E$ values between the E_{MP2} and the total $E_{SAPT2+(3)dMP2}$ energies (Table 3). The desirable SAPT components exhibited the same pattern of the energetic results of the considered complexes. For example, E_{elst} values of the SbF_5···, IF_3O_2···, and XeF_2O_3···NCH complexes were −42.50, −14.71, and −4.72 kcal/mol in a company with E_{int} values of −26.55, −7.04, and −2.84 kcal/mol, respectively.

https://doi.org/10.1021/acsomega.3c08178
ACS Omega 2024, 9, 10391−10399

CONCLUSIONS

σ-Hole site-based interactions between the hypervalent pnicogen, halogen, and aerogen-bearing molecules within the trigonal bipyramidal structure and pyridine/NCH LBs were minutely studied. For this purpose, ZF_5···, XF_3O_2···, and AeF_2O_3···LB complexes (where Z = As and Sb; X = Br and I; Ae = Kr and Xe; and LB = pyridine and NCH) were investigated. EP affirmations elucidated the ability of the inspected systems to form σ-hole with different magnitudes that increased according to the following order AeF_2O_3 < XF_3O_2 < ZF_5. Consistent with EP findings, the proficiency of σ-hole site-based interactions increased based on the atomic size of the central atom in the succeeding order: AeF_2O_3··· < XF_3O_2··· < ZF_5···pyridine/NCH complexes along with more favorability for the pyridine-based complexes over the NCH ones. Such preferentiality was attributed to the drastic deformation energies (i.e., geometrical deformation) that could be concluded as follows: (i) the drastic geometrical deformation of ZF_5 molecules from the trigonal bipyramidal geometry to the square pyramidal one upon complexation with the pyridine and NCH LBs; (ii) the notable E_{def} in the case of XF_3O_2···pyridine complexes rather than ···NCH counterparts; and (iii) the absence of geometrical deformation within most of the AeF_2O_3···pyridine and ···NCH complexes. QTAIM and NCI index affirmations admitted the partially covalent nature of most of the investigated complexes. Generally, SAPT indications outlined E_{elst} as the driving force beyond the occurrence of the considered interactions. Such outcomes will help in understanding the intermolecular interactions and will subsequently blaze a trail for the forthcoming applications in crystal engineering and biological systems.

AUTHOR INFORMATION

Corresponding Authors

Mahmoud A.A. Ibrahim − *Computational Chemistry Laboratory, Chemistry Department, Faculty of Science, Minia University, Minia 61519, Egypt; School of Health Sciences, University of KwaZulu-Natal, Westville Campus, Durban 4000, South Africa;* orcid.org/0000-0003-4819-2040; Email: m.ibrahim@compchem.net

Tamer Shoeib − *Department of Chemistry, The American University in Cairo, New Cairo 11835, Egypt;* orcid.org/0000-0003-3512-1593; Email: t.shoeib@aucegypt.edu

Authors

Asmaa M.M. Mahmoud − *Computational Chemistry Laboratory, Chemistry Department, Faculty of Science, Minia University, Minia 61519, Egypt*

Mohammed N.I. Shehata − *Computational Chemistry Laboratory, Chemistry Department, Faculty of Science, Minia University, Minia 61519, Egypt;* orcid.org/0000-0002-3334-6070

Rehab R.A. Saeed − *Computational Chemistry Laboratory, Chemistry Department, Faculty of Science, Minia University, Minia 61519, Egypt*

Nayra A.M. Moussa − *Computational Chemistry Laboratory, Chemistry Department, Faculty of Science, Minia University, Minia 61519, Egypt;* orcid.org/0000-0003-3712-7710

Shaban R.M. Sayed − *Department of Botany and Microbiology, College of Science, King Saud University, Riyadh 11451, Saudi Arabia*

Mohamed Khaled Abd El-Rahman − *Department of Chemistry and Chemical Biology, Harvard University, Cambridge, Massachusetts 02138, United States*

Complete contact information is available at: https://pubs.acs.org/10.1021/acsomega.3c08178

Author Contributions

M.A.A.I. contributed in the conceptualization, methodology, software, resources, project administration, supervision, and writing—review and editing. A.M.M.M. contributed in data curation, formal analysis, investigation, visualization, and writing—original draft. M.N.I.S. participated in methodology, investigation, project administration, and writing—review and editing. R.R.A.S. contributed in the methodology, investigation, project administration, and writing—review and editing. N.A.M.M. participated in the methodology, investigation, project administration, and writing—review and editing. S.R.M.S. is responsible for the resources and writing—review and editing. M.K.A.E.-R. participated in the writing—review and editing. T.S. contributed in the conceptualization, methodology, and writing—review and editing.

Notes

The authors declare no competing financial interest.

ACKNOWLEDGMENTS

The authors extend their appreciation to the Researchers Supporting Project No. (RSPD2024R743), King Saud University, Riyadh, Saudi Arabia, for funding this work. The computational work was performed with resources provided by the Science and Technology Development Fund (STDF-Egypt, grants nos. 5480 and 7972), Bibliotheca Alexandrina (http://hpc.bibalex.org), and The American University in Cairo. M.A.A.I. thanks the Center for High-Performance Computing (CHPC, www.chpc.ac.za), Cape Town, South Africa, for providing computational resources. M.A.A.I. extends his appreciation to the Academy of Scientific Research and Technology (ASRT, Egypt) for funding the Graduation Projects conducted at CompChem Lab, Egypt.

REFERENCES

(1) de la Cruz, X.; Reverter, J.; Fita, I. Representation of noncovalent interactions in protein structures. *J. Mol. Graph.* **1992**, *10*, 96−100.

(2) Ibrahim, M. A. A.; Shehata, M. N. I.; Moussa, N. A. M.; Hemia, R. R. A.; Abd Elhafez, H. S. M.; Abd El-Rahman, M. K.; Sayed, S. R. M.; Sidhom, P. A.; Dabbish, E.; Shoeib, T. Preferability of Molnupiravir, an Anti-COVID-19 Drug, toward Purine Nucleosides: A Quantum Mechanical Study. *ACS Omega* **2023**, *8*, 27553−27565.

(3) Yamakawa, M.; Yamada, I.; Noyori, R. CH/π Attraction: The Origin of Enantioselectivity in Transfer Hydrogenation of Aromatic Carbonyl Compounds Catalyzed by Chiralη6-Arene-Ruthenium(II) Complexes. *Angew. Chem., Int. Ed.* **2001**, *40*, 2818−2821.

(4) Luo, M. Chemical and Biochemical Perspectives of Protein Lysine Methylation. *Chem. Rev.* **2018**, *118*, 6656−6705.

(5) Bertani, R.; Sgarbossa, P.; Venzo, A.; Lelj, F.; Amati, M.; Resnati, G.; Pilati, T.; Metrangolo, P.; Terraneo, G. Halogen bonding in metal−organic−supramolecular networks. *Coord. Chem. Rev.* **2010**, *254*, 677−695.

(6) Mahmudov, K. T.; Gurbanov, A. V.; Guseinov, F. I.; Guedes da Silva, M. F. C. Noncovalent interactions in metal complex catalysis. *Coord. Chem. Rev.* **2019**, *387*, 32−46.

(7) Riley, K. E.; Hobza, P. Noncovalent interactions in biochemistry. *Wiley Interdiscip. Rev. Comput. Mol. Sci.* **2011**, *1*, 3−17.

(8) Varadwaj, P. R.; Varadwaj, A.; Marques, H. M.; Yamashita, K. Significance of hydrogen bonding and other noncovalent interactions

in determining octahedral tilting in the $CH_3NH_3PbI_3$ hybrid organic-inorganic halide perovskite solar cell semiconductor. *Sci. Rep.* **2019**, *9*, 50.
(9) Frieden, E. Non-covalent interactions. Keyto biological flexibility and specificity. *J. Chem. Educ.* **1975**, *52*, 754−756.
(10) Mahmudov, K. T.; Kopylovich, M. N.; Guedes da Silva, M. F. C.; Pombeiro, A. J. L. Chalcogen bonding in synthesis, catalysis and design of materials. *Dalton Trans.* **2017**, *46*, 10121−10138.
(11) Berger, G.; Robeyns, K.; Soubhye, J.; Wintjens, R.; Meyer, F. Halogen bonding in a multi-connected 1,2,2-triiodo-alkene involving geminal and/or vicinal iodines: a crystallographic and DFT study. *CrystEngComm* **2016**, *18*, 683−690.
(12) Saccone, M.; Cavallo, G.; Metrangolo, P.; Resnati, G.; Priimagi, A., Halogen-Bonded Photoresponsive Materials. In *Halogen Bonding II: Impact on Materials Chemistry and Life Sciences*, Metrangolo, P.; Resnati, G., Eds. Springer International Publishing: Cham, 2015; pp 147−166.
(13) Präsang, C.; Bruce, D. W. Halogen-Bonded Liquid Crystals. *Helv. Chim. Acta* **2023**, *106*, No. e202300008.
(14) Politzer, P.; Murray, J.; Janjić, G.; Zarić, S. σ-Hole Interactions of Covalently-Bonded Nitrogen, Phosphorus and Arsenic: A Survey of Crystal Structures. *Crystals* **2014**, *4*, 12−31.
(15) Scholfield, M. R.; Zanden, C. M.; Carter, M.; Ho, P. S. Halogen bonding (X-bonding): a biological perspective. *Protein Sci.* **2013**, *22*, 139−152.
(16) Kriz, K.; Fanfrlik, J.; Lepsik, M. Chalcogen Bonding in Protein-Ligand Complexes: PDB Survey and Quantum Mechanical Calculations. *ChemPhysChem* **2018**, *19*, 2540−2548.
(17) Murray, J. S.; Riley, K. E.; Politzer, P.; Clark, T. Directional Weak Intermolecular Interactions: σ-Hole Bonding. *Aust. J. Chem.* **2010**, *63*, 1598−1607.
(18) García-Llinás, X.; Bauzá, A.; Seth, S. K.; Frontera, A. Importance of R−CF3···O Tetrel Bonding Interactions in Biological Systems. *J. Phys. Chem. A* **2017**, *121*, 5371−5376.
(19) Jiang, S.; Zhang, L.; Cui, D.; Yao, Z.; Gao, B.; Lin, J.; Wei, D. The Important Role of Halogen Bond in Substrate Selectivity of Enzymatic Catalysis. *Sci. Rep.* **2016**, *6*, 34750−34756.
(20) Politzer, P.; Lane, P.; Concha, M. C.; Ma, Y.; Murray, J. S. An overview of halogen bonding. *J. Mol. Model.* **2007**, *13*, 305−311.
(21) Scheiner, S. Origins and properties of the tetrel bond. *Phys. Chem. Chem. Phys.* **2021**, *23*, 5702−5717.
(22) Bhattarai, S.; Sutradhar, D.; Chandra, A. K. Strongly Bound pi-Hole Tetrel Bonded Complexes between H_2SiO and Substituted Pyridines. Influence of Substituents. *ChemPhysChem* **2022**, *23*, No. e202200146.
(23) Ibrahim, M. A. A.; Moussa, N. A. M.; Kamel, A. A. K.; Shehata, M. N. I.; Ahmed, M. N.; Taha, F.; Abourehab, M. A. S.; Shawky, A. M.; Elkaeed, E. B.; Soliman, M. E. S. External Electric Field Effect on the Strength of sigma-Hole Interactions: A Theoretical Perspective in Likecdots, three dots, centeredLike Carbon-Containing Complexes. *Molecules* **2022**, *27*, 2963.
(24) Ibrahim, M. A. A.; Shehata, M. N. I.; Rady, A. S. M.; Abuelliel, H. A. A.; Abd Elhafez, H. S. M.; Shawky, A. M.; Oraby, H. F.; Hasanin, T. H. A.; Soliman, M. E. S.; Moussa, N. A. M. Effects of Lewis Basicity and Acidity on sigma-Hole Interactions in Carbon-Bearing Complexes: A Comparative Ab Initio Study. *Int. J. Mol. Sci.* **2022**, *23*, 13023.
(25) Bauza, A.; Mooibroek, T. J.; Frontera, A. Sigma-hole opposite to a lone pair: Unconventional pnicogen bonding interactions between ZF3 (Z = N, P, As, and Sb) compounds and several donors. *ChemPhysChem* **2016**, *17*, 1608−1614.
(26) Feng, G.; Evangelisti, L.; Gasparini, N.; Caminati, W. On the Cl···N halogen bond: a rotational study of CF_3Cl···NH_3. *Chemistry* **2012**, *18*, 1364−1368.
(27) Murray, J. S.; Lane, P.; Politzer, P. A predicted new type of directional noncovalent interaction. *Int. J. Quantum Chem.* **2007**, *107*, 2286−2292.
(28) Scheiner, S. The pnicogen bond: its relation to hydrogen, halogen, and other noncovalent bonds. *Acc. Chem. Res.* **2013**, *46*, 280−288.
(29) Blanco, F.; Alkorta, I.; Rozas, I.; Solimannejad, M.; Elguero, J. A theoretical study of the interactions of NF(3) with neutral ambidentate electron donor and acceptor molecules. *Phys. Chem. Chem. Phys.* **2011**, *13*, 674−683.
(30) Alkorta, I.; Elguero, J.; Del Bene, J. E. Exploring the PX3:NCH and PX3:NH3 potential surfaces, with X = F, Cl, and Br. *Chem. Phys. Lett.* **2015**, *641*, 84−89.
(31) Bhattarai, S.; Sutradhar, D.; Huyskens, T. Z.; Chandra, A. K. Nature and Strength of the π-Hole Chalcogen Bonded Complexes between Substituted Pyridines and SO3Molecule. *ChemistrySelect* **2021**, *6*, 7514−7524.
(32) Azofra, L. M.; Scheiner, S. Substituent Effects in the Noncovalent Bonding of SO(2) to Molecules Containing a Carbonyl Group. The Dominating Role of the Chalcogen Bond. *J. Phys. Chem. A* **2014**, *118*, 3835−3845.
(33) Varadwaj, P. R. Does Oxygen Feature Chalcogen Bonding? *Molecules* **2019**, *24*, 3166−3183.
(34) Wang, W.; Ji, B.; Zhang, Y. Chalcogen bond: A sister noncovalent bond to halogen bond. *J. Phys. Chem. A* **2009**, *113*, 8132−8135.
(35) Aakeroy, C. B.; Bryce, D. L.; Desiraju, G. R.; Frontera, A.; Legon, A. C.; Nicotra, F.; Rissanen, K.; Scheiner, S.; Terraneo, G.; Metrangolo, P.; Resnati, G. Definition of the chalcogen bond (IUPAC Recommendations 2019). *Pure Appl. Chem.* **2019**, *91*, 1889−1892.
(36) Ibrahim, M. A. A.; Saeed, R. R. A.; Shehata, M. N. I.; Moussa, N. A. M.; Tawfeek, A. M.; Ahmed, M. N.; Abd El-Rahman, M. K.; Shoeib, T. Sigma-Hole and Lone-Pair-Hole Site-Based Interactions of Seesaw Tetravalent Chalcogen-Bearing Molecules with Lewis Bases. *ACS Omega* **2023**, *8*, 32828−32837.
(37) Ibrahim, M. A. A.; Shehata, M. N. I.; Soliman, M. E. S.; Moustafa, M. F.; El-Mageed, H. R. A.; Moussa, N. A. M. Unusual chalcogen···chalcogen interactions in like···like and unlike Y = C=Y··· Y = C=Y complexes (Y = O, S, and Se). *Phys. Chem. Chem. Phys.* **2022**, *24*, 3386−3399.
(38) Zhou, F.; Liu, Y.; Wang, Z.; Lu, T.; Yang, Q.; Liu, Y.; Zheng, B. A new type of halogen bond involving multivalent astatine: an ab initio study. *Phys. Chem. Chem. Phys.* **2019**, *21*, 15310−15318.
(39) Bundhun, A.; Ramasami, P.; Murray, J. S.; Politzer, P. Trends in σ-hole strengths and interactions of F_3MX molecules (M = C, Si, Ge and X = F, Cl, Br, I). *J. Mol. Model.* **2013**, *19*, 2739−2746.
(40) Priimagi, A.; Cavallo, G.; Metrangolo, P.; Resnati, G. The halogen bond in the design of functional supramolecular materials: recent advances. *Acc. Chem. Res.* **2013**, *46*, 2686−2695.
(41) Desiraju, G. R.; Ho, P. S.; Kloo, L.; Legon, A. C.; Marquardt, R.; Metrangolo, P.; Politzer, P.; Resnati, G.; Rissanen, K. Definition of the halogen bond (IUPAC Recommendations 2013). *Pure Appl. Chem.* **2013**, *85*, 1711−1713.
(42) Ibrahim, M. A. A.; Saeed, R. R. A.; Shehata, M. N. I.; Ahmed, M. N.; Shawky, A. M.; Khowdiary, M. M.; Elkaeed, E. B.; Soliman, M. E. S.; Moussa, N. A. M. Type I−IV Halogen···Halogen Interactions: A Comparative Theoretical Study in Halobenzene···Halobenzene Homodimers. *Int. J. Mol. Sci.* **2022**, *23*, 3114.
(43) Bauza, A.; Frontera, A. π-Hole aerogen bonding interactions. *Phys. Chem. Chem. Phys.* **2015**, *17*, 24748−24753.
(44) Esrafili, M. D.; Asadollahi, S.; Vakili, M. Investigation of substituent effects in aerogen-bonding interaction between ZO_3(Z = Kr, Xe) and nitrogen bases. *Int. J. Quantum Chem.* **2016**, *116*, 1254−1260.
(45) Wang, R.; Liu, H.; Li, Q.; Scheiner, S. Xe···chalcogen aerogen bond. Effect of substituents and size of chalcogen atom. *Phys. Chem. Chem. Phys.* **2020**, *22*, 4115−4121.
(46) Politzer, P.; Murray, J. S.; Clark, T. Halogen bonding and other σ-hole interactions: A perspective. *Phys. Chem. Chem. Phys.* **2013**, *15*, 11178−11189.
(47) Bauza, A.; Frontera, A. Aerogen Bonding Interaction: A New Supramolecular Force? *Angew. Chem.* **2015**, *54*, 7340−7343.

https://doi.org/10.1021/acsomega.3c08178
ACS Omega 2024, 9, 10391−10399

(48) Grabarz, A.; Michalczyk, M.; Zierkiewicz, W.; Scheiner, S. Noncovalent bonds between tetrel atoms. *ChemPhysChem* **2020**, *21*, 1934−1944.
(49) Wang, X.; Li, B.; Li, Y.; Wang, H.; Ni, Y.; Wang, H. The influence of monomer deformation on triel and tetrel bonds between TrR_3/TR_4 (Tr = Al, Ga, In; T = Si, Ge, Sn) and N-base (N-base = HCN, NH3, CN^-). *Comput. Theor. Chem.* **2021**, *1201*, No. 113268.
(50) Michalczyk, M.; Zierkiewicz, W.; Wysokinski, R.; Scheiner, S. Hexacoordinated Tetrel-Bonded Complexes between TF4 (T = Si, Ge, Sn, Pb) and NCH: Competition between sigma- and pi-Holes. *ChemPhysChem* **2019**, *20*, 959−966.
(51) Zierkiewicz, W.; Wysokinski, R.; Michalczyk, M.; Scheiner, S. Chalcogen bonding of two ligands to hypervalent YF(4) (Y = S, Se, Te, Po). *Phys. Chem. Chem. Phys.* **2019**, *21*, 20829−20839.
(52) Scheiner, S.; Lu, J. Halogen, Chalcogen, and Pnicogen Bonding Involving Hypervalent Atoms. *Chem. - Eur. J.* **2018**, *24*, 8167−8177.
(53) Zierkiewicz, W.; Michalczyk, M.; Scheiner, S. Implications of monomer deformation for tetrel and pnicogen bonds. *Phys. Chem. Chem. Phys.* **2018**, *20*, 8832−8841.
(54) Frisch, M. J.; Trucks, G. W.; Schlegel, H. B.; Scuseria, G. E.; Robb, M. A.; Cheeseman, J. R.; Scalmani, G.; Barone, V.; Mennucci, B.; Petersson, G. A.; Nakatsuji, H.; Caricato, M.; Li, X.; Hratchian, H. P.; Izmaylov, A. F.; Bloino, J.; Zheng, G.; Sonnenberg, J. L.; Hada, M.; Ehara, M.; Toyota, K.; Fukuda, R.; Hasegawa, J.; Ishida, M.; Nakajima, T.; Honda, Y.; Kitao, O.; Nakai, H.; Vreven, T.; Montgomery, J. A.; Peralta, J. E.; Ogliaro, F.; Bearpark, M.; Heyd, J. J.; Brothers, E.; Kudin, K. N.; Staroverov, V. N.; Kobayashi, R.; Normand, J.; Raghavachari, K.; Rendell, A.; Burant, J. C.; Iyengar, S. S.; Tomasi, J.; Cossi, M.; Rega, N.; Millam, J. M.; Klene, M.; Knox, J. E.; Cross, J. B.; Bakken, V.; Adamo, C.; Jaramillo, J.; Gomperts, R.; Stratmann, R. E.; Yazyev, O.; Austin, A. J.; Cammi, R.; Pomelli, C.; Ochterski, J. W.; Martin, R. L.; Morokuma, K.; Zakrzewski, V. G.; Voth, G. A.; Salvador, P.; Dannenberg, J. J.; Dapprich, S.; Daniels, A. D.; Farkas, Ö.; Foresman, J. B.; Ortiz, J. V.; Cioslowski, J.; Fox, D. J. *Gaussian 09, Revision E01; Gaussian09*; Gaussian Inc.: Wallingford CT, USA., 2009.
(55) Møller, C.; Plesset, M. S. Note on an approximation treatment for many-electron systems. *Phys. Rev.* **1934**, *46*, 618−622.
(56) Woon, D. E.; Dunning, T. H. Gaussian basis sets for use in correlated molecular calculations. IV. Calculation of static electrical response properties. *J. Chem. Phys.* **1994**, *100*, 2975−2988.
(57) Woon, D. E.; Dunning, T. H. Gaussian basis sets for use in correlated molecular calculations. III. The atoms aluminum through argon. *J. Chem. Phys.* **1993**, *98*, 1358−1371.
(58) Feller, D. The role of databases in support of computational chemistry calculations. *J. Comput. Chem.* **1996**, *17*, 1571−1586.
(59) Ibrahim, M. A. A. Molecular mechanical perspective on halogen bonding. *J. Mol. Model.* **2012**, *18*, 4625−4638.
(60) Piela, L. *Ideas of quantum chemistry*. Elsevier: 2006.
(61) Boys, S. F.; Bernardi, F. The calculation of small molecular interactions by the differences of separate total energies. Some procedures with reduced errors. *Mol. Phys.* **1970**, *19*, 553−566.
(62) Grabowski, S. J.; Sokalski, W. A. Different types of hydrogen bonds: correlation analysis of interaction energy components. *J. Phys. Org. Chem.* **2005**, *18*, 779−784.
(63) Bader, R. F. W. Atoms in molecules. *Acc. Chem. Res.* **1985**, *18*, 9−15.
(64) Johnson, E. R.; Keinan, S.; Mori-Sanchez, P.; Contreras-Garcia, J.; Cohen, A. J.; Yang, W. Revealing noncovalent interactions. *J. Am. Chem. Soc.* **2010**, *132*, 6498−6506.
(65) Lu, T.; Chen, F. Multiwfn: a multifunctional wavefunction analyzer. *J. Comput. Chem.* **2012**, *33*, 580−592.
(66) Humphrey, W.; Dalke, A.; Schulten, K. VMD: Visual molecular dynamics. *J. Mol. Graph.* **1996**, *14*, 33−38.
(67) Hohenstein, E. G.; Sherrill, C. D. Density fitting and Cholesky decomposition approximations in symmetry-adapted perturbation theory: Implementation and application to probe the nature of π-π interactions in linear acenes. *J. Chem. Phys.* **2010**, *132*, 184111−184120.
(68) Turney, J. M.; Simmonett, A. C.; Parrish, R. M.; Hohenstein, E. G.; Evangelista, F. A.; Fermann, J. T.; Mintz, B. J.; Burns, L. A.; Wilke, J. J.; Abrams, M. L.; Russ, N. J.; Leininger, M. L.; Janssen, C. L.; Seidl, E. T.; Allen, W. D.; Schaefer, H. F.; King, R. A.; Valeev, E. F.; Sherrill, C. D.; Crawford, T. D. PSI4: An open-source ab initio electronic structure program. *Wiley Interdiscip. Rev. Comput. Mol. Sci.* **2012**, *2*, 556−565.
(69) Parker, T. M.; Burns, L. A.; Parrish, R. M.; Ryno, A. G.; Sherrill, C. D. Levels of symmetry adapted perturbation theory (SAPT). I. Efficiency and performance for interaction energies. *J. Chem. Phys.* **2014**, *140*, No. 094106.
(70) Al-Wahaibi, L. H.; Chakraborty, K.; Al-Shaalan, N. H.; Majeed, M. Y. A. S.; Blacque, O.; Al-Mutairi, A. A.; El-Emam, A. A.; Percino, M. J.; Thamotharan, S. Quantitative analysis of hydrogen and chalcogen bonds in two pyrimidine-5-carbonitrile derivatives, potential DHFR inhibitors: an integrated crystallographic and theoretical study. *RSC Adv.* **2020**, *10*, 36806−36817.
(71) Arnold, W. D.; Oldfield, E. The chemical nature of hydrogen bonding in proteins via NMR: J-couplings, chemical shifts, and AIM theory. *J. Am. Chem. Soc.* **2000**, *122*, 12835−12841.
(72) Jablonski, M. Bond paths between distant atoms do not necessarily indicate dominant interactions. *J. Comput. Chem.* **2018**, *39*, 2183−2195.
(73) Jablonski, M. On the Uselessness of Bond Paths Linking Distant Atoms and on the Violation of the Concept of Privileged Exchange Channels. *ChemistryOpen* **2019**, *8*, 497−507.
(74) Otero-de-la-Roza, A.; Johnson, E. R.; Contreras-Garcia, J. Revealing non-covalent interactions in solids: NCI plots revisited. *Phys. Chem. Chem. Phys.* **2012**, *14*, 12165−12172.
(75) Jeziorski, B.; Moszynski, R.; Szalewicz, K. Perturbation-theory approach to intermolecular potential-energy surfaces of van der Waals complexes. *Chem. Rev.* **1994**, *94*, 1887−1930.

https://doi.org/10.1021/acsomega.3c08178
ACS Omega 2024, 9, 10391−10399